Soft Robotic Proprioception Enhancement via 3D-Printed Differential Optical Waveguide Design

Shaowu Tang, *Graduate Student Member, IEEE*, Kailuan Tang, *Graduate Student Member, IEEE*, Yutao Guo, Shijian Wu, Jiahao Xu, Benkang Lou, Sicong Liu, *Member, IEEE*, Juan Yi, Jian S. Dai, *Fellow, IEEE*, and Zheng Wang, *Senior Member, IEEE*

***Abstract*—Soft robots undergo complex deformations during actuation and interaction due to the flexibility and compliance of their soft materials. This characteristic presents challenges in proprioception, particularly in characterizing their spatial deformations. Soft optical waveguide sensors have emerged as a reliable solution for soft robotic proprioception owing to their compact form factor that enables ease of integration into the soft body, and their high sensitivity in detecting deformations. In this study, we introduce a differential optical waveguide design that combines light-blocking and light-transmitting structures featured with distinct light attenuation, leading to monotonically variable sensing signals in response to bidirectional deformation. Consequently, this design enables the differentiation of two directions of deformation using merely one sensor. We employ three-dimensional printing technology and adjust printing parameters to tune the attenuation of both structures and accommodate various deformation modes, including proprioceptive bidirectional bending, shearing, and twisting. Furthermore, the sensing capabilities can also be extended to cope with deformation in three dimensions, based on the combinations of differential optical waveguides. The proposed method is validated through design, simulations, fabrication, and experiments. Finally, a differential optical waveguide is integrated into a dual-chamber soft actuator showcasing the performance in detecting the bidirectional bending motion. This developed methodology offers design guidance for soft optical sensors and may inspire the development of integration of sensing in soft robots capable of complex motion.**

***Index Terms*—Soft robotics, soft sensors, optical waveguide, bidirectional deformation, proprioception.**

Manuscript received 30 January 2024; accepted 1 June 2024. Date of publication 19 June 2024; date of current version 26 June 2024. This letter was recommended for publication by Associate Editor V. Ho and Editor C. Laschi upon evaluation of the reviewers' comments. This work was supported in part by the NSFC under Grant 52105021 and in part by Shenzhen Science, Tech. & Innovation Commission under\penalty -\@M Grant ZDSYS20220527171403009 and Grant RCBS20210609104446099. *(Corresponding author: Juan Yi.)*

Shaowu Tang and Jian S. Dai are with the Shenzhen Key Laboratory of Intelligent Robotics and Flexible Manufacturing Systems, Southern University of Science and Technology, Shenzhen 518000, China, and also with the Department of Mechanical and Energy Engineering, Southern University of Science and Technology, Shenzhen 518000, China (e-mail: 12232306@mail.sustech.edu.cn).

Kailuan Tang is with the School of Mechatronics Engineering, Harbin Institute of Technology, Harbin 150001, China, and also with the Department of Mechanical and Energy Engineering, Southern University of Science and Technology, Shenzhen 518000, China (e-mail: tangkl@mail.sustech.edu.cn).

Yutao Guo, Shijian Wu, Jiahao Xu, Benkang Lou, Sicong Liu, and Zheng Wang are with the Department of Mechanical and Energy Engineering, Southern University of Science and Technology, Shenzhen 518000, China (e-mail: 12132305@mail.sustech.edu.cn).

Juan Yi is with the Shenzhen Key Laboratory of Intelligent Robotics and Flexible Manufacturing Systems, Southern University of Science and Technology, Shenzhen 518000, China, also with the Department of Mechanical and Energy Engineering, Southern University of Science and Technology, Shenzhen 518000, China, and also with the College of Mechatronics and Control Engineering, Shenzhen University, Shenzhen 518000, China (e-mail: yijuan2603@outlook.com).

This letter has supplementary downloadable material available at https://doi.org/10.1109/LRA.2024.3416795, provided by the authors.

Digital Object Identifier 10.1109/LRA.2024.3416795

I. Introduction

SOFT robotics has attracted interest and gained widespread attention in recent years. Benefitting from the utilization of soft materials, soft robots exhibit high compliance and flexibility, allowing them to accomplish diverse tasks in unstructured environments [1]. However, this inherent compliance also leads to continuous and complex soft robotic body deformations, thus presenting challenges in proprioception that provide important feedback information for controlling soft robots [2], [3].

Soft strain sensors have been widely explored with various sensing mechanisms, involving resistive, capacitive, and magnetic sensing methods, showing the possibility of capturing the continuous soft body deformations by locally embedding them within soft robots [4], [5], [6], [7], [8], while maintaining compliance and adaptability in soft robots. To capture more complex deformations and spatially multidirectional motion, such as spatial bending, shearing, or twisting, researchers have dedicated considerable efforts to integrating various sensing mechanisms into a single compact sensor [9], [10] or distributing multiple soft sensors across the soft body [11], [12], [13]. These efforts emphasize the use of redundant sensory inputs to acquire more deformation information and improve proprioception through the implementation of sensor morphology and learning-based techniques. Among these sensing mechanisms, optical is an interesting and classic sensing method in soft robots due to its high sensitivity, fast response, lower hysteresis, and easy integration [14], [15], [16], [17], [18].

Optical waveguide sensors designed based on total internal reflection have been used to characterize multiple deformation modes [19], [20], [21], [22], [23], [24], [25], [26]. More recently, research on optical sensing also exhibits high information-rich characteristics [27], [28], with the chromaticity and intensity of light decoded from a single light input to multiple outputs, enabling multimodal information measurement through a simple sensor design. Innovative sensor designs with smart optical waveguide structures including lace network [29], orb web [30], microchannel [31] and off-centered fiber [32] have also been studied to effectively minimize redundancy while acquiring multimodal sensory information. These efforts on optical sensing highly demonstrated the promising perspectives for facilitating the simplified design and information processing,

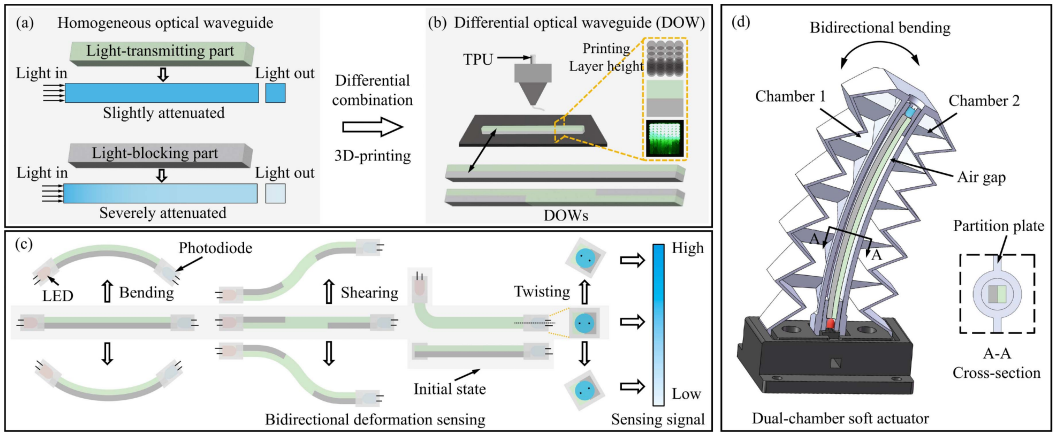

Fig. 1. Concept of DOW on design, fabrication, and application. (a) Light propagates through the light-transmitting and light-blocking waveguides. (b) The DOW is fabricated integrally using the 3D-printing method with a single TPU material. The light attenuation of the light-blocking and light-transmitting parts is simply adjusted by changing printing parameters, including the number of serial segments and the layer height. (c) Three types of DOW-based deformation sensors (for bending, shearing, and twisting). (d) The bidirectional bending sensor is integrated into a dual-chamber soft actuator.

especially with the advancements in three-dimensional (3D) printing technologies, thus worthy of in-depth investigation.

In this research, we further explore the potential of utilizing optical mechanism with simple and information-rich design for sensing complex deformations in soft robotics. in particular, we propose a method of a differential optical waveguide (DOW) design, which comprises light-blocking and light-transmitting parts with distinct light attenuation. These parts are designed to guide the propagation of light within the waveguide, leading to variations in light irradiance as the soft robot deforms in different directions. Building upon this differential combination design and 3D-printing fabrication technology, we also propose a method to adjust the light attenuation characteristics of the waveguide through two parameters: the number of serial segments and the layer height. Consequently, by utilizing a combination of various light-blocking and light-transmitting parts, the DOW can be fabricated using a single TPU (Thermoplastic Polyurethane) soft material, and bidirectional deformation (e.g. bending, shearing, and twisting) can be sensed and characterized through one sensor set (one light-emitting diode (LED) and photodiode). This DOW design can also be extended by combining several light-transmitting and light-blocking parts to sense omnidirectional deformation. The core concept, design, fabrication, and experimental validation are explained, contributing to the deformation sensing of omnidirectional bending and integration of sensing into a soft dual-chamber actuator. The main contributions of this work are as follows:

1) Proposing the concept of DOW design, which can guide light to propagate within a waveguide through the combination of light-blocking and light-transmitting parts, enabling the characterization of bidirectional deformation by a single sensing signal.
2) Proposing the 3D-printing fabrication method for adjusting the light attenuation of waveguide through two printing parameters: the number of serial segments and the layer height, resulting in integrated printing of DOWs with both light-blocking and light-transmitting parts using merely one TPU material. These DOWs can be utilized to characterize the bidirectional bending, shearing, and twisting deformation with specific combinations of these parts.
3) Demonstrating the multi-DOW sensor design enabling omnidirectional bending sensing as well as the integrated soft robot design featuring a dual-chamber soft actuator and sensor, which validates the proposed approach with a comprehensive methodology that includes the differential optical sensing concept, design, fabrication, and experimental validation.

II. Concept

The concept of DOW design we proposed consists of light-blocking and light-transmitting parts to guide the propagation of light within the waveguide, thereby enabling bidirectional deformation sensing through only one sensing signal. Specifically, for homogeneous waveguides with different light attenuation, light is attenuated to varying degrees when propagating in them as shown in Fig. 1(a). Based on this understanding, we aim to differentially combine these light-blocking and light-transmitting parts, to guide the propagation state of light within the waveguide. Fortunately, by employing 3D-printing methods with a single TPU material, the light attenuation of the waveguide can be readily adjusted through simple changes of printing parameters or structural design as shown in Fig. 1(b), so that the DOWs with light-blocking and light-transmitting parts can be fast and low-cost fabricated.

As shown in Fig. 1(c), bidirectional deformation sensors are composed of a DOW, an LED, and a photodiode, which have different sensing signals when deforming in opposite directions. Taking the bidirectional bending sensor as an example, in its initial state, approximately half of the light enters the light-transmitting part and the other half enters the light-blocking part; when it bends to the light-blocking part from the initial state, more light enters outside of the light-transmitting ring from the light-blocking (details in Fig. 2(b), so that the sensing signal increases. In contrast, when it bends to the light-transmitting part, the sensing signal decreases.

With their soft bodies, the DOW sensors can be integrated into soft robots with high coherence. As is shown in Fig. 1(d), to demonstrate their capabilities, a bending sensor was integrated into a dual-chamber soft actuator for proprioception.

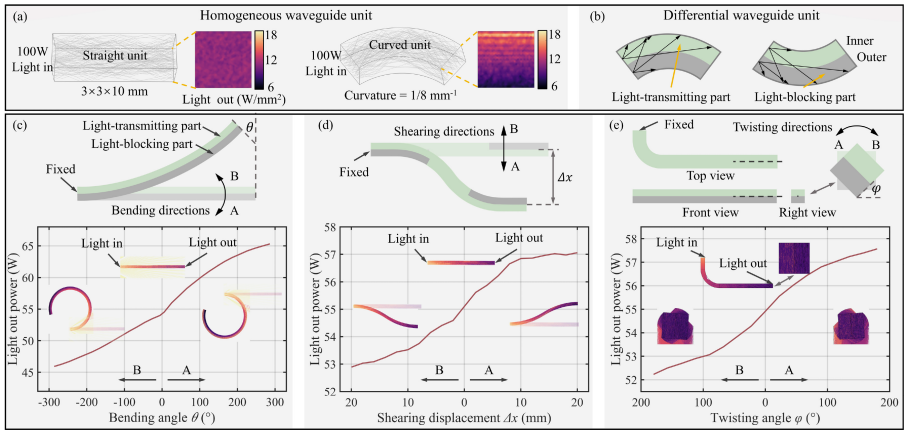

Fig. 2. Propagation and distribution of light in waveguides. (a) Finite element analysis (FEA) of light propagation in homogeneous straight and curved waveguide units. (b) Light propagates in DOW units. FEA of (c) bending-DOW, (d) shearing-DOW, and (e) twisting-DOW.

III. Design and Fabrication

A. Working Principle

The characteristics of the light attenuation [33] in waveguides are crucial to the design of the Differential Optical Waveguide (DOW) proposed in this letter. The working principle will be introduced and verified through simulations (COMSOL Ray Optics) from two aspects: the propagation characteristics of light in homogeneous optical waveguides and in differential optical waveguides.

Firstly, the simulations of two homogeneous waveguides shown in Fig. 2(a) include a straight waveguide unit, which is a cuboid with dimensions of 3 × 3 ×10 mm, clad in air. Infrared light with a divergence angle of 36° (940 nm, 100 W power) is input from the left side, and frozen calculated at the right side. The conditions for the other simulation model remain the same, except for a curvature of 1/8 mm^{-1}. The simulation results show the distribution of light irradiance on the right side of both units: the radiation is uniform in the straight unit, whereas in the curved unit, the outer ring exhibits higher irradiance than the inner ring. This non-uniform distribution in the curved waveguide unit underlies the design of the DOW. As shown in Fig. 2(b), the upper portion of the waveguide is designed as the light-transmitting part and the lower portion as the light-blocking part. Therefore, this whole waveguide with its differential light attenuation structure, allows light to propagate under varying conditions, resulting in distinct responses to deformations and their directions.

Then, by utilizing different combinations of the light-blocking and light-transmitting parts, we designed three types of DOWs, namely bending-DOW, shearing-DOW, and twisting-DOW. Their structures and simulation results for deformation are shown in Fig. 2(c)–2(e). In terms of dimensions: the bending-DOW is 3 ×3 × 100 mm, with the light-blocking part being 1.5 mm in height; the shearing-DOW is also 3× 3 × 100 mm, with each light-blocking section being 1.5 ×3 × 40 mm; and the twisting-DOW is L-shaped, with a cross-section of 3 × 3 mm, a long side of 80 mm, a short side of 20 mm, and rounded corner with a radius of 10 mm. In terms of boundary conditions: the three DOWs are subjected to bending, shearing, and twisting deformations respectively, in two opposite directions denoted as A and B (see Fig. 2(c)–2(e)); the attenuation coefficients of light-transmitting and light-blocking parts are 0.5 m^{-1} and 10 m^{-1}, respectively; the input light power is 100 W; the output optical powers are collected and calculated. Fig. 2(c)–2(e) also present the simulation results of the DOWs' responses to their deformation. The output powers of the three DOWs increase when deformed towards direction A and decrease when deformed towards direction B. These simulation results validate the feasibility of the DOWs design and will serve as a critical basis for the development of deformation sensors.

TABLE I
Printing Parameters of DOW

Layer Height	0.08 - 0.3 mm	Shells	4
Nozzle diameter	0.4 mm	Extrusion Width	0.38 mm
Printing Speed	25 mm/s	Extruder temperature	220°C

B. Light Attenuation of 3D-Printed Waveguide

The main principle of DOWs is that they comprise parts with different light attenuation to adjust the output power of light during deformation. Therefore, before the fabrication of DOWs, the discussion of the light attenuation of the 3D-printed waveguide is necessary. In this letter, we utilize the FDM 3D-printing method (implemented by Raise 3D Pro2, Raise 3D Technologies, Inc.), and a transparent soft printing material (eTPU-95 A clear, Esun Industrial Co., Ltd.) to fabricate the optical waveguides.

To adjust the light attenuation of the 3D-printed waveguide, two simple ways are proposed, as shown in Fig. 3(a) and 3(d), which involve the number of serial segments and the printing layer height of the waveguide respectively. For the first way, we utilize slits (0.001 mm width) to segment the waveguide (3 × 3 × 100 mm) in its CAD model. These slits will automatically guide the 3D-printing path when the segmented waveguide is sliced by the commercially available software (ideaMaker, Raise3D), as shown in Fig. 3(a). The key aspect is that these slits will be filled during the actual printing process, and it is these laterally guided printing paths that block the light propagation in the axial direction of the waveguide. The main slicing parameters are listed in Table I. In particular, the "shells" parameter in idearMaker is set to 4, ensuring that the sliced printing path consists of only straight lines arranged parallel to the waveguide axis, thereby facilitating light propagation within the waveguide.

Although light attenuation is a crucial coefficient for designing DOWs, it does not require direct measurement but is reflected by comparing the received light irradiance at the left-end of each

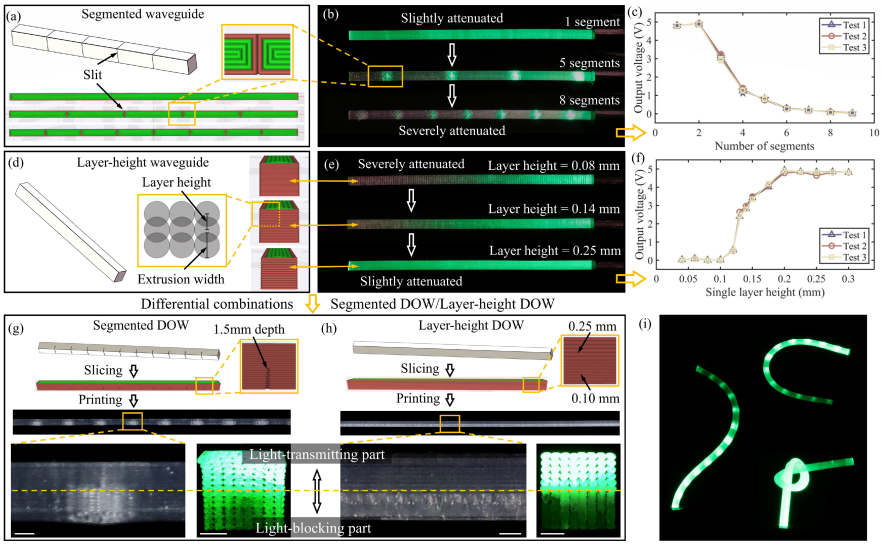

Fig. 3. Design and fabrication of DOWs. (a) The CAD and sliced model of the segmented waveguide. The light attenuation increases with the number of segments in (b)-(c). (d)-(f) The layer height in printing is the other parameter to adjust light attenuation; as it increases, light attenuation decreases. (g)-(h) The differential combination of waveguides, including both segmented and layer-height DOWs. The scale bar is 1 mm. (i) The DOWs have good flexibility.

waveguide when its right-end has the same light power input. Fig. 3(b) shows the effect of the slit-guided printing path on waveguide's light attenuation. The visible green light propagates well from right to left when there are no slit in the waveguide, and the brightness at left-end gradually diminishes as the number of slits increases. Furthermore, a quantitative comparison of waveguide attenuation is shown in Fig. 3(c). Results of three repeated tests indicate that the output voltage decreases as the number of segments increases. This suggests that segmentation is a useful way for adjusting light attenuation, which increases with the number of segments.

Printing layer height is another factor to adjust the light attenuation of 3D-printed optical waveguides. Due to the characteristics of fused deposition, there will be overlap between layers in the 3D-printing path when slice parameters "Layer Height" is smaller than "Extrusion Width" as shown in Fig. 3(d). Consequently, on the one hand, a smaller printing layer height results in more overlapping areas, thus reducing the transparency and increasing light attenuation of the printed waveguide. On the other hand, a smaller printing layer height leads to more printing layers, which increases the printing time for the same object and may introduce more random defects in the printed waveguide caused by nozzle temperature changes or motor rotation errors. Therefore, we printed waveguides with layer height ranging from 0.04 mm to 0.3 mm and explored the effect of printed layer height on light attenuation. The results are shown in Fig. 3(e) and 3(f), which illustrate that the attenuation decreases with increasing printing layer height.

So far, we have described the fabrication method of 3D-printed waveguides and have also proposed and validated two ways to adjust light attenuation of light-blocking and light-transmitting parts. These will be an important basis for designing DOW.

C. Differential Optical Waveguide

Based on two light attenuation tuning methods mentioned above, in this section, we will present the design and fabrication of Segmented Differential Optical Waveguide (SDOW) and Layer-Height Differential Optical Waveguide (HDOW).

Fig. 3(g) shows the CAD and sliced model of SDOW, using 1-segment and 11-segment differential waveguide as an example. The lower part of the waveguide contains ten slits with a width of 0.001 mm and a depth of 1.5 mm, while the upper part does not have any slit. This SDOW can be printed in 11 min by using a simple slit design.

To print HDOW, the key is to add a "Per-Layer Setting" in slicing software. Taking HDOW in Fig. 3(h) as an example, we set the parameter of printing layer height to 0.10 mm when the Z-axis is from 0 mm to 1.5 mm, and 0.25 mm when Z-axis from 1.5 mm to 3 mm. The slicing software automatically generates a 6 min printing path and contains 15 layers with a height of 0.10 mm and 6 layers with a height of 0.25 mm.

The waveguides shown in Fig. 3(g) and (h) were printed by segmented and layer-height methods, respectively, and details and differences of light-blocking and light-transmitting parts were shown in the lateral and cross-sectional views as well. When visible green light enters the waveguide, it can be observed that the bright and dark parts from the other end (photographed by a digital microscope), which verifies that the light-blocking part and the light-transmitting part play a role in guiding the propagation of light. Concomitantly, there is a 0.175 mm (5.8% to total height) transitioning region when switching between different layer heights. The influence of this region on the waveguide characteristics is not considered in this work.

In addition, as they are entirely fabricated from TPU soft material, the waveguides exhibit good flexibility in deformations, as shown in Fig. 3(i), and thus are well-suited for integration with soft robots.

IV. Experimental Validation

Based on the simulation results and 3D-printing fabrication method of DOWs, we designed three types of bidirectional deformation sensors, including bending, shearing, and twisting

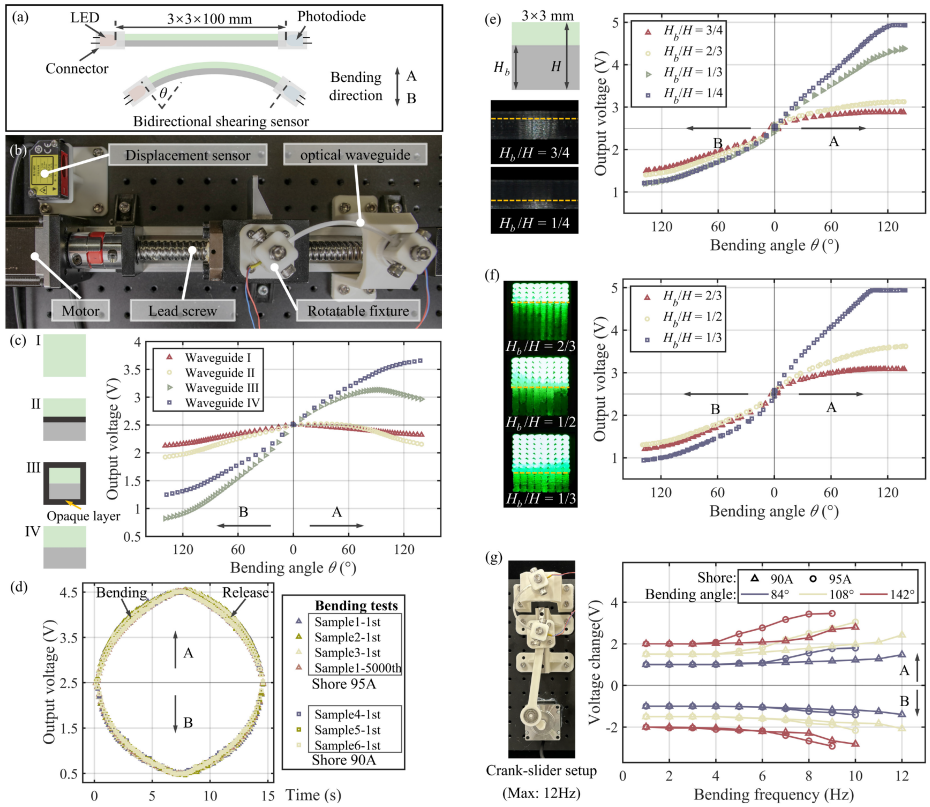

Fig. 4. Experiments and results of the bending sensor. (a) The structure of the bending sensor. (b) The experimental setup for bending tests. (c) Four waveguide designs are compared. (d) The repeatability and consistency of the sensor. (e)-(f) The effects of proportion ratio on sensor's performance. (g) The dynamic response of the sensor.

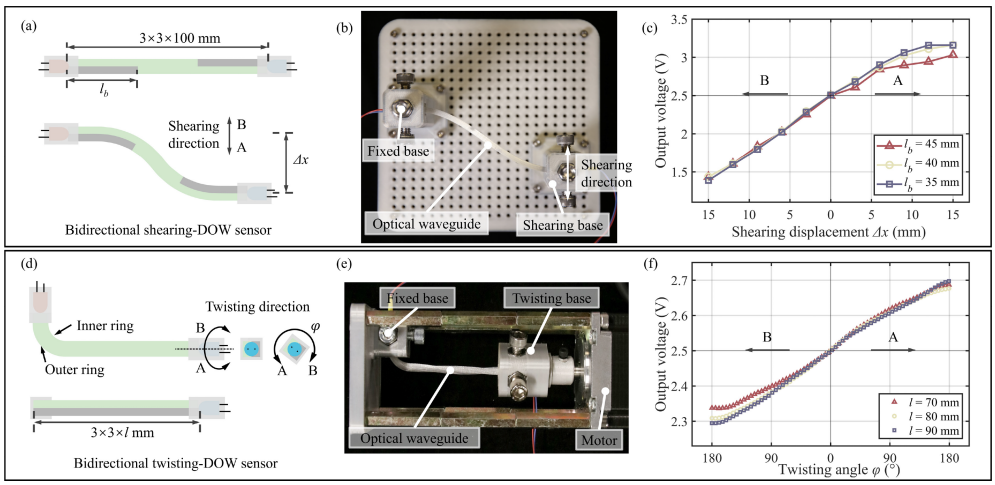

Fig. 5. The structure, experimental setup, and results of the shearing sensor (a)-(c), and the twisting sensor (d)-(e).

sensor. The structure of these sensors is not complicated, as shown in Figs. 4(a) and 5(a)(d). All of them consist of a waveguide, an LED, a photodiode (wavelength 940 nm, TSAL4400 and TEFT4300, respectively, Vishay Intertechnology, Inc.), and two connectors. Combined with a simple peripheral circuit, the sensor outputs a 0∼5 V voltage when the photodiode receives light irradiance from LED [13]. This output voltage is the main parameter used to explore the sensor characteristics in this letter. Next, we will conduct experiments to evaluate the characteristics and performance of these three types of DOW sensors.

A. *Bidirectional Bending-DOW Sensor*

For the bidirectional bending-DOW sensor, as shown in Fig. 4(a), the waveguide size is 3 × 3 × 100 mm, and θ is defined as the bending angle. The experimental setup for investigating

the characteristics of the bidirectional bending-DOW sensors is shown in Fig. 4(b). The connectors at both ends are fixed to two rotatable fixtures, with the right fixture immovable and the left fixture horizontally movable. A rotating DC motor drives the horizontal movement of the sliding table and left fixture through a lead screw. The linear displacement is recorded by a laser sensor (HG-C1200, Panasonic), which is mounted on a base plate. As two rotatable fixtures get closer, the waveguide is forced to bend. In this setup, bending experiments in directions A and B are performed separately, and the sensing voltage generated by the photodiode and peripheral circuits is recorded.

To validate the uniqueness of the DOW sensor we proposed, a total of four waveguide designs were first tested for their characteristics. Fig. 4(c) shows the cross-sections of these waveguides (I-IV), where green denotes the light-transmitting part with a printing layer-height of 0.25 mm; gray represents the light-blocking part with a printing layer-height of 0.10 mm; and black signifies opaque layer (0.4 mm thickness black double-sided tape), which light can barely pass through due to its absorption and reflection. The other dimensions of the four waveguides are identical. Fig. 4(c) also shows experimental results of these four waveguides in bidirectional bending when θ ranges from 0° to 138°. To ensure a uniform comparison, the initial voltage signal of each sensor was set to 2.5 V by adjusting the peripheral circuit. From the results, the voltage signal received by homogeneous waveguide I decreases from 2.5 V to 2.32 V when bending in A direction and to 2.13 V when bending in B direction. For the separated differential optical waveguide II, light propagation is prohibited between the light-blocking and light-transmitting parts, and the results exhibit similar characteristics to waveguide I, with a decrease in the sensing signal in both directions, the minimum voltage observed when bending in the A direction is 2.15 V and in the B direction, it is 1.92 V. For the surrounded differential optical waveguide III, light propagation is permitted between the light-transmitting and light-blocking parts. In the bending direction A, the received voltage first increases gradually, reaching a maximum value of 3.13 V at a bending angle θ of 92.5°, and then decreases gradually to 2.97 V. In the bending direction B, as bending angle θ increases, the voltage signal decreases rapidly, with a minimum value of 0.82 V, which is 67.2% lower than the initial voltage. The differential optical waveguide IV exhibited unique characteristics in the bending experiment. Its voltage signal increases monotonically when bending in direction A and decreases monotonically in direction B. This result confirms the feasibility of the proposed DOW design, as it allows the full characterization of bidirectional bending deformation with only one sensing signal.

To verify the repeatability and consistency of the DOW sensor, we assessed the bending characteristics of 6 samples. Samples 1–3 were fabricated from 95 A TPU material (eTPU-95 A clear, Esun), while samples 4–6 were made from 90 A TPU material (PolyFlex TPU90 clear, Polymaker). Fig. 4(d) shows the 1st bending results of 6 samples and the 5000th bending results of sample 1. Each bending test lasted 14.5 seconds which can be considered a quasi-static process. Following the linear calibration of the test data (where the voltage is 2.5 V at 0° and 4.5 V at 138°), the voltage change curves for each sensor in both the A and B directions are nearly identical. Among these results, in the A bending direction, there is the largest difference between sample 3 and sample 4, with an RMSE of 0.104 V. This result confirms the repeatability and stability of the DOW sensor.

Then, to regulate the performance of the DOW sensors by structural parameters, we investigated the effect of the proportion ratio on the characteristics of the bending-DOW sensor. in Fig. 4(e), H_b/H represents the proportion ratio of the height of light-blocking part to the total height of waveguide, which is set to 1/4, 1/3, 2/3, and 3/4 in SDOW, and 1/3, 1/2, and 2/3 in HDOW as shown in Fig. 4(e) and (f). From the results, on the one hand, the proportion ratio significantly influences the sensing signal. Specifically, as the proportion ratio decreases, the variation range of the voltage signal increases. For instance, in SDOW with H_b/H of 3/4, the voltage signal ranges from 1.49 V to 2.88 V, whereas in SDOW with H_b/H of 1/4, it ranges from 1.21 V to 4.92 V. On the other hand, due to the limitations of the photodiode, there is a saturation value for sensing voltage, approximately 5 V. For SDOW with H_b/H of 1/4, at a bending angle of 121.1°, received voltage reached the saturation value of 4.92 V; for HDOW with H_b/H of 1/3, at a bending angle of 103.4°, the received voltage reaches the saturation value of 4.93 V. In addition to the saturation value of the photodiode, the characteristics of the waveguide itself also lead to non-linearity of the sensing, with the waveguide a maximum of 2.84 V for SDOW with H_b/H of 3/4. The proposed DOW is supposed to bidirectionally characterize deformation using only one sensing signal. Therefore, SDOW with H_b of 1/3 and HDOW with H_b/H of 1/2 are deemed ideal. These results will guide us in adjusting the proportion ratio of the light-blocking part of to ensure the bidirectional bending-DOW sensor operates within an appropriate range and state.

Finally, to showcase the dynamic performance, we dynamically tested the sensor with bending frequencies from 1 Hz to 12 Hz, on the crank-slider setup shown in Fig. 4(g). Waveguides with hardness ratings of 90 A and 95 A were subjected to bending tests at angles ranging from 0° to 84°, 0° to 108°, and 0° to 142°. The average voltage changes during the bending process were recorded. From the results, on the one hand, the sensing signal remains relatively stable at low bending frequencies. As the frequency increases, the inertia of waveguides influences their bending deformation, causing instability in the sensing signal. On the other hand, the waveguide's hardness significantly impacts its dynamic performance, with higher hardness resulting in greater stability. For example, in the dynamic response of the waveguide bending towards direction A in the 0° to 142° range, the bandwidth of the 90 A waveguide is about 5 Hz, whereas the bandwidth of the 95 A waveguide is about 9 Hz.

B. Bidirectional Shearing-DOW Sensor

For the bidirectional shearing-DOW sensor, the waveguide size is also 3 $\times$ 3 $\times$ 100 mm. As the waveguide forms two continuous arcs with opposite curvature directions during shear deformation, two light-blocking parts are arranged within the waveguide as shown in Fig. 5(a), with a length of l_b and a height of 1.5 mm. This design aims for the shearing deformation to be bidirectionally characterized by a single sensing signal from the photodiode.

The sensors with light-blocking part lengths l_b of 35 mm, 40 mm, and 45 mm were tested in Fig. 5(b). The sensor connectors were mounted on two bases: the left base was fixed, and the right base was manually moved and secured with bolts before each measurement. In this setup, the shear displacement Δx of the right base in A and B directions, and sensing voltage are recorded. From the results, the voltage signal increases

monotonically when shearing in direction A and decreases monotonically when shearing in direction B. These results verify that our proposed DOW sensor design can clearly distinguish the shear deformation of the waveguide in both directions. On the other hand, the length of the light-blocking part has less influence on sensor characteristics, especially shearing in direction B, the three voltage signals almost overlap and decrease from 2.5 V to about 1.4 V.

C. Bidirectional Twisting-DOW Sensor

For the bidirectional twisting-DOW sensor, to construct bending inner and outer rings with different light attenuation during twisting deformation, the waveguide is designed as an L-shape, with the long side of 80 mm, the short side of 20 mm, and the rounded corner with a radius of 10 mm, as shown in Fig. 5(d). When the waveguide twists toward direction A, the upper light-transmitting part is rotated to the outer ring, allowing the photodiode to receive more light. Conversely, when it twists in direction B, more light enters the blocking outer ring and is severely attenuated. Therefore, the twisting deformation could also be characterized bidirectionally.

Three bidirectional twisting-DOW sensors with long side lengths of 70 mm, 80 mm, and 90 mm are experimented with in setup as shown in Fig. 5(e). The short side of the L-shaped waveguide is fixed, and the long side is coaxial with the motor's shaft. During these tests, the waveguides were twisted from 0° to 180° in both clockwise and counterclockwise directions, and the twisting angle φ and sensing voltage were recorded. The results in Fig. 5(f) verified that these sensors can directionally distinguish and characterize twisting deformation and are nearly unaffected by their length. However, the sensing signal range of twisting-DOW sensors is the smallest compared to bending-DOW and shearing-DOW sensors. From the initial state of 2.5 V to the maximum of 2.7 V (twisting 180° in direction A) and the minimum of 2.3 V (twisting 180° in direction B), the sensing signal only increases and decreases by 0.2 V respectively.

D. Demonstrations on Omnidirectional Bending-DOW Sensor

Using 3D-printing technology, it is straightforward to fabricate omnidirectional deformable optical waveguides by designing various combinations of light-blocking parts and light-transmitting parts. Here, an omni-bending DOW is used for demonstration. The cross-sectional diameter of the omni-bending DOW is 8 mm, and its length is 120 mm. It features a regular triangular prism light-blocking part (10 segments) at the center and a light-transmitting part (1 segment) surrounding it, as shown in Fig. 6(a). An LED is located at the left end of the sensor, emitting 940 nm infrared light, and three photodiodes are located at the right end to collect signals at different positions.

Bending tests in three principle directions of A, B, and C were conducted, bending angles ranging from 0 ° to 50 °. The test results are shown in Fig. 6(b). When bending in direction A, more light enters the side of photodiode 1, increasing sensing signal 1. The three sensing signals have significant differences in deformation in different directions. These results show that our DOW design has the potential for omnidirectional deformation perception.

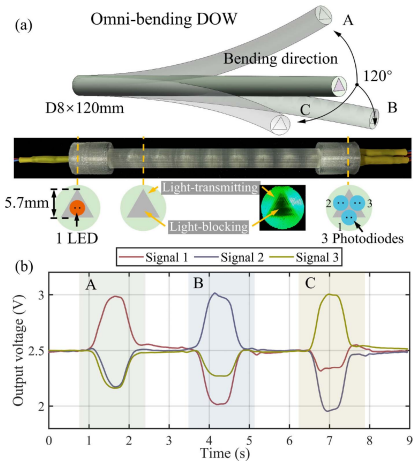

Fig. 6. Demonstration on the omni-bending DOW sensor. (a) The structure of the omni-bending DOW. (b) Test results of the omni-bending DOW sensor.

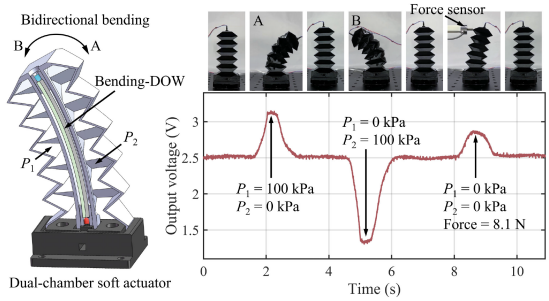

Fig. 7. Demonstration of proprioceptive and contact sensing on a soft actuator with an integrated sensor..

E. Demonstrations on Soft Actuator With an Integrated Sensor

The purpose of proprioception in soft robots is to determine their body posture or deformation when they are actively actuated or passively interacting with the environment. To demonstrate the proprioceptive sensing capability of our DOW design, a bidirectional bending-DOW sensor was integrated into a dual-chamber soft actuator, as shown in Fig. 7. The DOW sensor deforms in synchronization with the soft actuator, which can bend in both directions when unequal pressure inputs are applied to the left and right chambers.

The demonstrations were conducted from two aspects, on the one hand, for the active actuation (0∼7 seconds), the pressure in the left and right chambers gradually increases from 0 kPa to 100 kPa and then decreases, respectively. The sensing signal over time during this experiment was recorded. When the robot system is not activated, the sensing voltage remains at 2.5 V. When the robot bends to the right, the sensing voltage increases monotonically to 3.12 V (with the left chamber pressure $P_1 =$ 100 kPa and the right chamber pressure $P_2 = 0$ kPa); conversely, when the robot bending to the left, the induced voltage decreases to 1.34 V (with the left chamber pressure at $P_1 = 0$ kPa and the right chamber pressure at $P_2 = 100$ kPa). On the other hand, during contact with the environment (7∼10 seconds), the air pressure in the two chambers is at 0 kPa, and the actuator is subjected to an external horizontal rightward contact force

ranging from 0 to 8.1 N. The sensing voltage monotonically rises to 2.86 V. The results from both aspects of the demonstrations illustrate that the proposed DOW sensor has good proprioception sensing capabilities.

V. Conclusion

In this work, we proposed a concept of differential optical waveguide (DOW) design that combines light-blocking and light-transmitting parts. When the waveguide bends, the light would be more concentrated on the outer side compared to the inner side. These sides consist of different parts with different light attenuation coefficients, i.e., the light-blocking and light-transmitting structures. This unique feature enables the bidirectional motion measurement using only one sensor set (one LED and photodiode). This concept was validated through simulations where the proposed differential optical waveguide was modelled to bend, shear, and twist in two directions, showing contrasting signal variation tendencies. Leveraging 3D printing technology, we fabricated and tested three waveguide designs capable of measuring bending, shearing, and twisting motions. The results showed that the deformation of these sensors can be characterized bidirectionally. Furthermore, by extending the combinations of light-blocking and light-transmitting parts, omnidirectional deformable optical waveguides can be easily produced. Related experimental results demonstrated that the DOW design possesses the potential for omnidirectional deformation sensing. To showcase the potential applications of the DOW design in soft robots, we implemented the bending sensor in a dual-chamber soft actuator. This demonstrated that bidirectional actuation states and contact states could be captured using just one sensor, highlighting the practicality and versatility of the DOW design.

In the future, the combination of light-blocking and light-transmitting parts will be further expanded, the multi-model proprioceptive and contact sensors will be investigated; The frustrated total internal reflection mechanism when the sensors contact with other soft structures will be explored, and a general analytical model of differential optical waveguides will be established; those sensors will be integrated on soft robotic systems, and the sensing signals will be calibrated for closed-loop control.

References

[1] D. Rus and M. T. Tolley, "Design, fabrication and control of soft robots," *Nature*, vol. 521, no. 7553, pp. 467–475, 2015.

[2] R. F. Shepherd et al., "Multigait soft robot," *Proc. Nat. Acad. Sci.*, vol. 108, no. 51, pp. 20400–20403, 2011.

[3] H. Wang et al., "Toward perceptive soft robots: Progress and challenges," *Adv. Sci.*, vol. 5, no. 9, 2018, Art. no. 1800541.

[4] R. L. Truby et al., "Soft somatosensitive actuators via embedded 3D printing," *Adv. Mater.*, vol. 30, no. 15, 2018, Art. no. 1706383.

[5] A. Atalay et al., "Batch fabrication of customizable silicone-textile composite capacitive strain sensors for human motion tracking," *Adv. Mater. Technol.*, vol. 2, no. 9, 2017, Art. no. 1700136.

[6] D. Hu et al., "Stretchable e-skin and transformer enable high-resolution morphological reconstruction for soft robots," *Nature Mach. Intell.*, vol. 5, no. 3, pp. 261–272, 2023.

[7] M. Luo et al., "Toward modular soft robotics: Proprioceptive curvature sensing and sliding-mode control of soft bidirectional bending modules," *Soft Robot.*, vol. 4, no. 2, pp. 117–125, 2017.

[8] C. Hegde et al., "Sensing in soft robotics," *ACS Nano*, vol. 17, no. 16, pp. 15277–15307, 2023.

[9] T. Kim et al., "Heterogeneous sensing in a multifunctional soft sensor for human-robot interfaces," *Sci. Robot.*, vol. 5, no. 49, 2020, Art. no.eabc6878.

[10] M. Totaro et al., "Integrated simultaneous detection of tactile and bending cues for soft robotics," *Soft Robot.*, vol. 4, no. 4, pp. 400–410, 2017.

[11] R. L. Truby, C. D. Santina, and D. Rus, "Distributed proprioception of 3D configuration in soft, sensorized robots via deep learning," *IEEE Robot. Automat. Lett.*, vol. 5, no. 2, pp. 3299–3306, Apr. 2020.

[12] A. A. Calderón et al., "An earthworm-inspired soft robot with perceptive artificial skin," *Bioinspiration Biomimetics*, vol. 14, no. 5, 2019, Art. no. 56012.

[13] Z. Shen et al., "Soft origami optical-sensing actuator for underwater manipulation," *Front. Robot. AI*, vol. 7, 2021, Art. no. 616128.

[14] C. Larson et al., "Highly stretchable electroluminescent skin for optical signaling and tactile sensing," *Science*, vol. 351, no. 6277, pp. 1071–1074, 2016.

[15] J. Jung, M. Park, D. Kim, and Y.-L. Park, "Optically sensorized elastomer air chamber for proprioceptive sensing of soft pneumatic actuators," *IEEE Robot. Automat. Lett.*, vol. 5, no. 2, pp. 2333–2340, Apr. 2020.

[16] R. B. N. Scharff, G. Fang, Y. Tian, J. Wu, J. M. P. Geraedts, and C. C. L. Wang, "Sensing and reconstruction of 3-D deformation on pneumatic soft robots," *IEEE/ASME Trans. Mechatronics*, vol. 26, no. 4, pp. 1877–1885, Aug. 2021.

[17] C. Li et al., "Highly robust and soft biohybrid mechanoluminescence for optical signaling and illumination," *Nature Commun.*, vol. 13, no. 1, 2022, Art. no. 3914.

[18] P. Zhang et al., "Integrated 3D printing of flexible electroluminescent devices and soft robots," *Nature Commun.*, vol. 13, no. 1, 2022, Art. no. 4775.

[19] H. Zhao et al., "Optoelectronically innervated soft prosthetic hand via stretchable optical waveguides," *Sci. Robot.*, vol. 1, no. 1, 2016, Art. no. eaai 7529.

[20] C. To, T. Hellebrekers, J. Jung, S. J. Yoon, and Y. -L. Park, "A soft optical waveguide coupled with fiber optics for dynamic pressure and strain sensing," *IEEE Robot. Automat. Lett.*, vol. 3, no. 4, pp. 3821–3827, Oct. 2018.

[21] K. C. Galloway et al., "Fiber optic shape sensing for soft robotics," *Soft Robot.*, vol. 6, no. 5, pp. 671–684, 2019.

[22] Y. Guo et al., "Soft and stretchable polymeric optical waveguide-based sensors for wearable and biomedical applications," *Sensors*, vol. 19, no. 17, 2019, Art. no. 3771.

[23] Z. Yang, S. Ge, F. Wan, Y. Liu, and C. Song, "Scalable tactile sensing for an omni-adaptive soft robot finger," in *Proc. IEEE 3rd Int. Conf. Soft Robot.*, 2020, pp. 572–577.

[24] H. Krauss and K. Takemura, "Stretchable optical waveguide sensor capable of two-degree-of-freedom strain sensing mediated by a semidivided optical core," *IEEE/ASME Trans. Mechatronics*, vol. 27, no. 4, pp. 2151–2157, Aug. 2022.

[25] J. Zhou et al., "Conformable and compact multiaxis tactile sensor for human and robotic grasping via anisotropic waveguides," *Adv. Mater. Technol.*, vol. 7, no. 11, 2022, Art. no. 2200595.

[26] L. Mo et al., "A multidirectional external perception soft actuator based on flexible optical waveguide for underwater teleoperation," *Adv. Intell. Syst.*, vol. 5, no. 10, 2023, Art. no. 2300029.

[27] R. Baines et al., "Multi-modal deformation and temperature sensing for context-sensitive machines," *Nature Commun.*, vol. 14, no. 1, 2023, Art. no. 7499.

[28] H. Bai et al., "Stretchable distributed fiber-optic sensors," *Science*, vol. 370, no. 6518, pp. 848–852, 2020.

[29] P. A. Xu et al., "Optical lace for synthetic afferent neural networks," *Sci. Robot.*, vol. 4, no. 34, 2019, Art. no. eaaw6304.

[30] A. Leal-Junior et al., "Multifunctional flexible optical waveguide sensor: On the bioinspiration for ultrasensitive sensors development," *Opto- Electron. Adv.*, vol. 5, no. 10, 2022, Art. no. 210098.

[31] D. Fan et al., "Innervation of sensing microchannels for Three-Dimensional stimuli perception," *Adv. Mater. Technol.*, vol. 8, no. 17, 2023, Art. no. 2300185.

[32] J. Ge, A. E. James, L. Xu, Y. Chen, K. -W. Kwok, and M. P. Fok, "Bidirectional soft silicone curvature sensor based on off-centered embedded fiber Bragg grating," *IEEE Photon. Technol. Lett.*, vol. 28, no. 20, pp. 2237–2240, Oct. 2016.

[33] S. Chang and A. K. Bowden, "Review of methods and applications of attenuation coefficient measurements with optical coherence tomography," *J. Biomed. Opt.*, vol. 24, no. 9, 2019, Art. no. 090901.